The 3D failure process in polymeric syntactic foams with different cenosphere volume fractions

Ruoxuan Huang [a], Peifeng Li [b,] *, Tong Liu [c], Jiujun Xu [a]

[a] Key Lab of Ship-Machinery Maintenance & Manufacture, Dalian Maritime University, Dalian 116026, China

[b] School of Engineering, University of Glasgow, Glasgow G12 8QQ, UK

[c] Singapore Institute of Manufacturing Technology, Singapore 637662, Singapore

* Correspondence to: Peifeng Li (peifeng.li@glasgow.ac.uk; Tel: +44 141 330 2703).

Abstract

The previous work (Huang and Li, Compos. Part B, 2015) proposed the failure mechanism in syntactic foams with low and high hollow microsphere volume fractions, based on the finite element simulation of localised stresses in the foam. In this work, in-situ X-ray microtomography of uniaxial compression tests was performed to provide the direct experimental evidence to the proposed mechanism by tracking the internal 3D failure process in epoxy syntactic foams with different cenosphere volume fractions (V). It was found that for both the low and high V, micro-cracks initiate in the matrix in the top and bottom of crushed cenospheres where the tensile stress concentrates, and then propagate longitudinally to become macro-cracks. Increasing the cenosphere volume fraction also leads to the formation of matrix micro-cracks in the connection zone where the stress concentrates significantly; the matrix micro-cracks thus propagate diagonally and longitudinally in the high V foam.

Keywords: Syntactic foam; Matrix cracking; Failure analysis; CT analysis.

1 Introduction

Polymeric syntactic foams have been widely used in load bearing components and buoyancy units due to their excellent properties including good chemical resistance, high specific strength, long durability and excellent energy dissipation capacity. Their applications can be found in automotive, aerospace, marine and construction sectors [1-3]. Embedded hollow microspheres strongly determine the overall properties of syntactic foams. Thus, various types of hollow microspheres have been reported in the previous studies, such as glass [4,5], polymeric [6], carbon [7] and ceramic [8] microspheres. Among them, glass microballoons are the most prevalent and have attracted considerable attention in industry. However, the continued effort is made on new candidates of hollow microspheres with lower cost and better performance.

Cenospheres, the byproduct of coal combustion, are ceramic hollow microspheres with small wall thickness to diameter ratio [9]. The low cost and the low bulk density make the cenosphere an ideal choice for developing lightweight syntactic foams [10,11]. A number of studies have been reported on the mechanical properties of cenosphere syntactic foams including tensile, compressive and flexural strengths, fracture, impact resistance, damping, and creep [10-14]. The syntactic foam is a special composite material with hollow microspheres being the additives (fillers). Rule of mixture can be used to quantitatively estimate some properties of the foam such as the elastic modulus and strength from the properties of the constituents [15]. Therefore, the content of the fillers has a strong influence on the overall behaviour of the syntactic foam. In particular, the effect of hollow microsphere volume fractions has been investigated on the bulk mechanical properties of syntactic foams at the quasi-static and dynamic loading rates [4,16-19].

The failure mechanism in the constituents of syntactic foams is an important factor determining the bulk behaviour such as the plateau strength and impact energy dissipation capacity. It is thus necessary to understand the failure process in order to optimise the design of the foam. Under quasi-static compressive loading, three main failure modes have been identified in polymeric syntactic foams: (i) shear fracture in the diagonal of the specimen (nearly 45° to the loading axis) [20], (ii) longitudinal splitting failure along the loading direction [21], (iii) layered crushing resulting from failure of some specific weak planes in the transverse direction [22]. The influencing factors of the failure process include the aspect ratio of specimens, the properties of constituents and the applied loading rates. It was recently documented that failure modes depend on the surface quality of syntactic foams (e.g., painted, coated or not) [23]. Under dynamic compression, the failure usually initiates at one side of the specimen, and cracks propagate to cut through the whole sample [24]. The volume fraction of hollow microspheres can also significantly affect the failure mechanism in the foam that consequently determines the bulk behaviour [4,19]. Our previous work elucidated and proposed the possible internal cracking failure in the matrix of glass microballoon epoxy syntactic foams based on 3D finite element (FE) modelling [4]. However, there is still lack of experimental evidence on the internal 3D damage process and the associated failure in syntactic foams with low and high volume fraction of hollow microspheres.

Most existing experimental work analysed the failure mechanism based on the surface features in failed specimens after mechanical testing [5,20,22,25,26]. However, such post-test inspections may not be able to reveal all the internal damages. Therefore, the insightful failure analysis relies on real-time examinations in 3D. The developments in X-ray microtomography (μXT) allow for the 3D observations of internal microstructural features in materials with the high spatial resolution. μXT has been the

powerful non-destructive testing tool to characterise composite materials with complex internal structures [27-29]. Various types of loading devices have recently been designed to perform in-situ μXT imaging on mechanical testing [12,30,31]. The in-situ experiments can track the structural changes in materials in different length scales.

The aim of this study was to investigate the effect of cenosphere volume fractions (V) on the failure process, especially the matrix failure in epoxy syntactic foams. In-situ μXT of uniaxial compression tests was performed on the syntactic foam specimens with low (V = 0.10) and high (V = 0.45) cenosphere volume fractions. The stress field in the syntactic foams as a function of glass microballoon volume fractions as predicted in the FE model in the previous work [4] was used to further understand the failure in the matrix.

2 Experimental procedure

2.1 Fabrication of syntactic foams

The syntactic foams were fabricated by mechanically mixing the cenospheres and the epoxy resin. CENOSTAR ES500 (CENOSTAR Corp., MA, USA) cenospheres were the fillers and Epicote 1006A epoxy resin was the matrix. Table 1 lists the chemical compositions and typical physical properties of the cenosphere, which were provided by the manufacturer. Two types of syntactic foams were prepared with the volume fraction of cenospheres V = 0.10 and V = 0.45. The fabrication process, as detailed for the similar syntactic foam in the reference [12,13], involved the following steps: (1) the cenospheres were gradually added into the epoxy resin and at the same time the mixture was stirred slowly until it became the uniform slurry; (2) the slurry was left in the vacuum oven for 10 minutes to reduce the gas bubbles introduced in the stirring

process; (3) the slurry was subsequently cast in the aluminium mould coated with the release agent and cured at room temperature for 24 hours; (4) the foam materials were taken out of the mould and machined into the specimens with the required dimensions.

Table 1 Chemical composition and physical properties of ES500 cenospheres.

Parameter *	Value
Composition (wt%)	Silica: 50–60
	Alumina: 22–30
	Iron: 1.5–5.0
Bulk density (kg m^{-3})	320–450
Outer diameter (μm)	150–499, 10%–25%
	105–149, 10%–30%
	75–104, 18%–30%
	45–74, 5%–20%
	<44, 2%–10%

2.2 Mechanical testing

Uniaxial compression experiments were performed on the syntactic foam specimens to measure the bulk stress–strain curves at the quasi-static rate. Cylindrical foam specimens of the diameter 10 mm and the aspect ratio 1:1 were tested in the INSTRON 5569 (INSTRON, MA, USA) electromechanical universal testing machine in conjunction with a 50 kN load cell at room temperature. Prior to testing, the two ends of each specimen were lubricated with the Castrol LMX grease to minimise the interfacial friction during compression. The crosshead speed was 0.6 mm min^{-1}, equivalent to the strain rate of 0.001 s^{-1} in the specimens. At least five specimens of each cenosphere volume fraction were tested in the same conditions.

2.3 In-situ X-ray microtomography of compression tests

X-ray microtomography was used to characterise the internal 3D microstructure of the cylindrical syntactic foam specimens of the diameter 3 mm and the length 3 mm. The specimen was sandwiched between two anvils in an in-house compression rig made of polycarbonate [12], and compressed to different deformation stages. The deformation was controlled at the strains of ε = 0, 0.1, 0.2, 0.35, and 0.5. After each strain step, the foam specimen together with the loading rig was scanned in the μXT system at the voltage 60 kV and the current 37 μA to track the morphological change in the microstructure. The 3D images were reconstructed with an approximate voxel size of 4 μm, and then visualised in the AVIZO/FIRE software. Details on the loading rig and in-situ μXT procedure can be found in the previous work [12].

3 Results and discussion

3.1 Microstructure of syntactic foams

The filtering algorithms were applied to process the reconstructed X-ray microtomographic images and clearly represent the internal 3D microstructure of the cenosphere epoxy syntactic foams (Fig. 1). The two constituents in the microstructure can be identified from the different greyscale values of the images. The white rings in the μXT slices are the walls of cenospheres; inside the cenospheres is the air pore represented by the black colour. The grey phase between black and white is the epoxy matrix. The cenospheres are randomly and uniformly distributed in the matrix (Fig. 1); thus the microstructure of the foam is homogeneous.

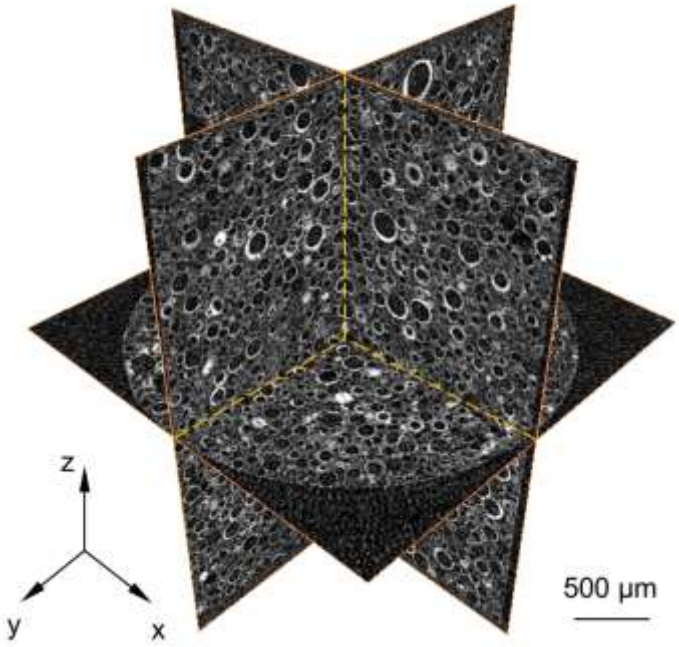

Fig. 1 Three orthogonal X-ray microtomographic slices showing the microstructure of the epoxy syntactic foam with the cenosphere volume fraction V = 0.45.

3.2 Stress–strain behaviour of the foam

The bulk stress–strain curves of the epoxy syntactic foams with different cenosphere volume fractions were calculated from the measured load and displacement histories in the uniaxial compression tests in the INSTRON machine (Fig. 2). The curves can be divided into the initial elastic, plateau and final densification regions, as in many other foam materials [32-34]. Despite the similar shape, the dissimilarity exists in the stress–strain curves of the foam specimens with the low and high cenosphere volume fractions. As shown in Fig. 2, the Young's modulus and initial peak stress increase as more cenospheres are added in the foam (i.e., increasing the volume fraction of cenospheres). This implies that the CENOSTAR ES500 cenosphere is the reinforcement constituent to the elastic behaviour of the epoxy syntactic foam. A large

deformation (strain) exists in the plateau region of the high V foam as crushed cenospheres produce more space to be consumed before densification.

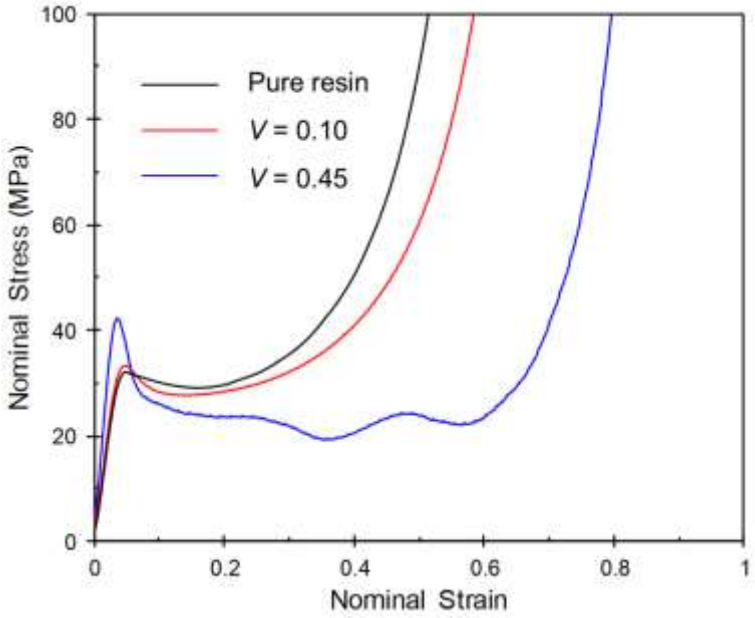

Fig. 2 Representative nominal stress–strain curves of syntactic foams with low and high cenosphere volume fractions under quasi-static compression.

3.3 In-situ observations of the failure process in the foam

Figs. 3 and 4 illustrate the μXT observations of the morphological evolution of microstructure in the syntactic foams (with the cenosphere volume fractions V = 0.10 and V = 0.45, respectively) at different deformation stages during the uniaxial compression. The failure process is dominated by crushing of cenospheres as well as the plastic deformation and fracture of the matrix [12]. The two failure processes can be considered the damage in the bulk foam [13]. The damage zones are highlighted from the intact zones in the foams (Figs. 3 and 4).

For both the epoxy syntactic foams with V = 0.10 and V = 0.45, the failure process initiates in the centre of the specimens where most of large cenospheres are compressed into to oblate spheroids and then crushed (refer to the strain ε = 0.1 in Figs. 3 and 4).

The substantial hydrostatic stress is responsible to the damage in the centre of the syntactic foam, according to the previous work [5].

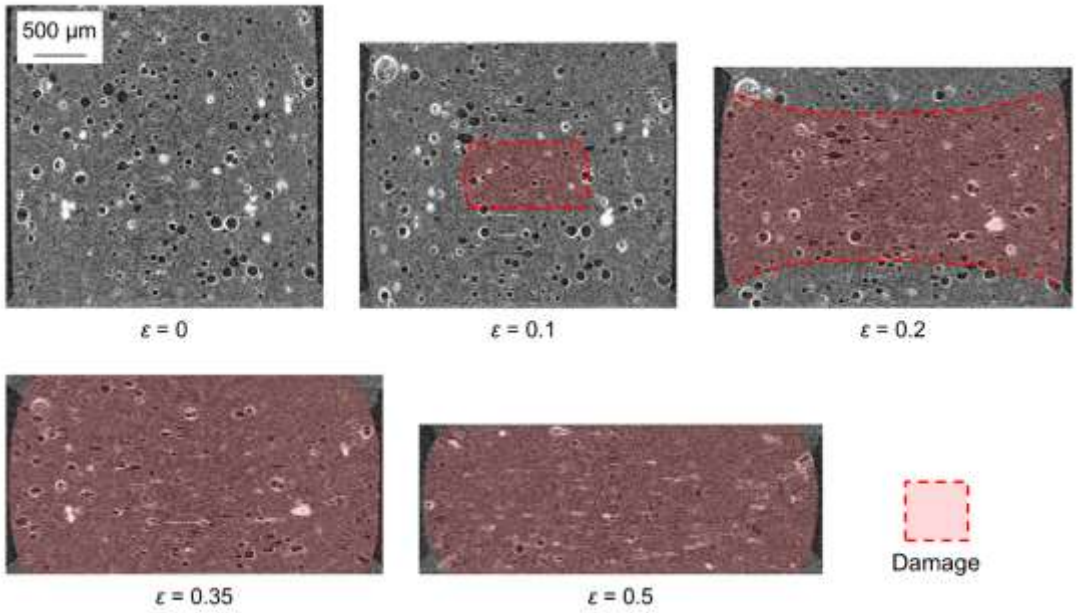

Fig. 3 An epoxy syntactic foam with the cenosphere volume fraction $V = 0.10$: X-ray microtomographic longitudinal slices of the internal deformation and failure process at different strain stages of the quasi-static compression.

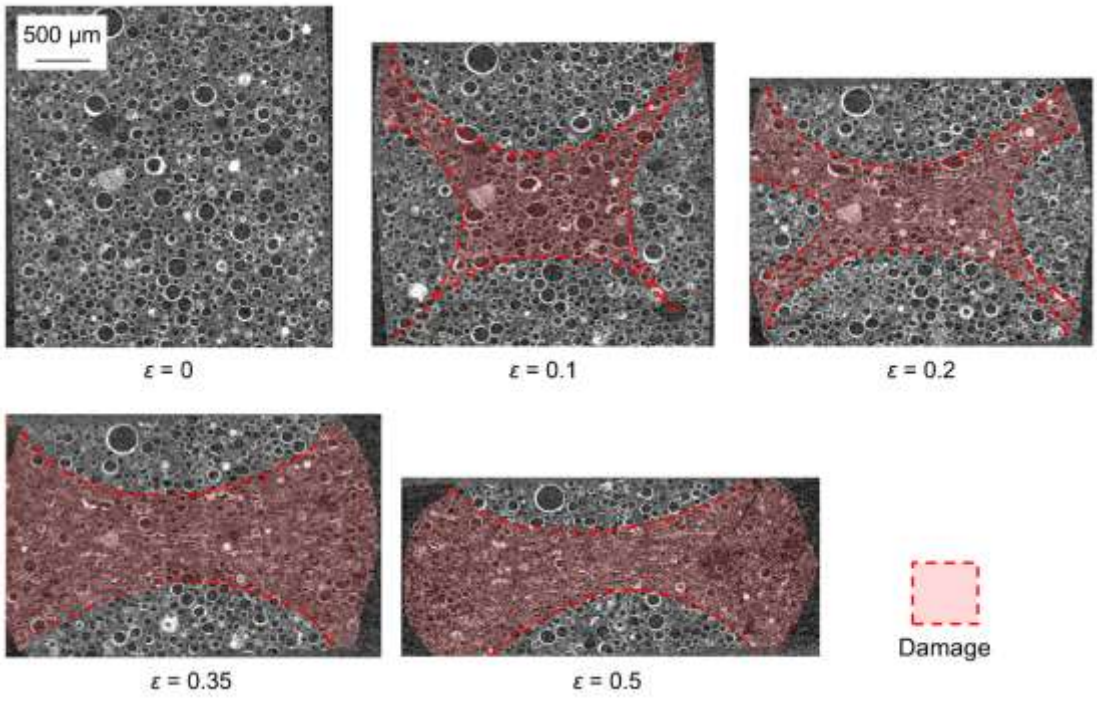

Fig. 4 An epoxy syntactic foam with the cenosphere volume fraction $V = 0.45$: X-ray microtomographic longitudinal slices of the internal deformation and failure process at different strain stages of the quasi-static compression.

The barrelling effect under further loading raises the shear stress along the diagonal in the foam specimen [5,35]. In the foam with the low cenosphere volume fraction ($V = 0.10$), cenospheres in the transverse (lateral) and longitudinal (vertical) directions are crushed under further compression. The damage zone expands in all directions, especially in the lateral direction ($\varepsilon = 0.2$ in Fig. 3). Almost all the cenospheres are then fractured at higher strains $\varepsilon = 0.35$ and 0.5 (refer to Fig. 3). The damage evolves throughout the low $V = 0.10$ foam specimen, leading to the densification.

The different failure process occurs in the foam with high cenosphere content ($V = 0.45$) subjected to further loading. Even though the damage evolves in all directions, the collapse of cenospheres in the diagonal is dominant as observed in the foam ($\varepsilon = 0.1$ and 0.2 in Fig. 4). The damage zone expands preferentially nearly 45° to the loading direction, i.e., along the maximum shear stress direction in the cylindrical foam specimen. Under further loads, the damage then evolves towards both the longitudinal and transverse directions ($\varepsilon = 0.35$ and 0.5 in Fig. 4). The two intact zones remain in the top and bottom of the foam specimen until the foam is densified at higher strain (densification strain approximately equal to 0.7 in Fig. 2).

3.4 Macroscopic failure in the matrix

To further reveal the failure of the matrix, the typical μXT transverse slices were selected from the top and centre of the syntactic foam specimens at the late stage of deformation ($\varepsilon = 0.5$). Fig. 5 illustrates not only the distribution of micro-cracks, but

also the macro-cracks that micro-cracks grow into. Both the damage and intact zones are also schematically shown for the foams with low (Fig. 5(b)) and high (Fig. 5(e)) cenosphere volume fractions.

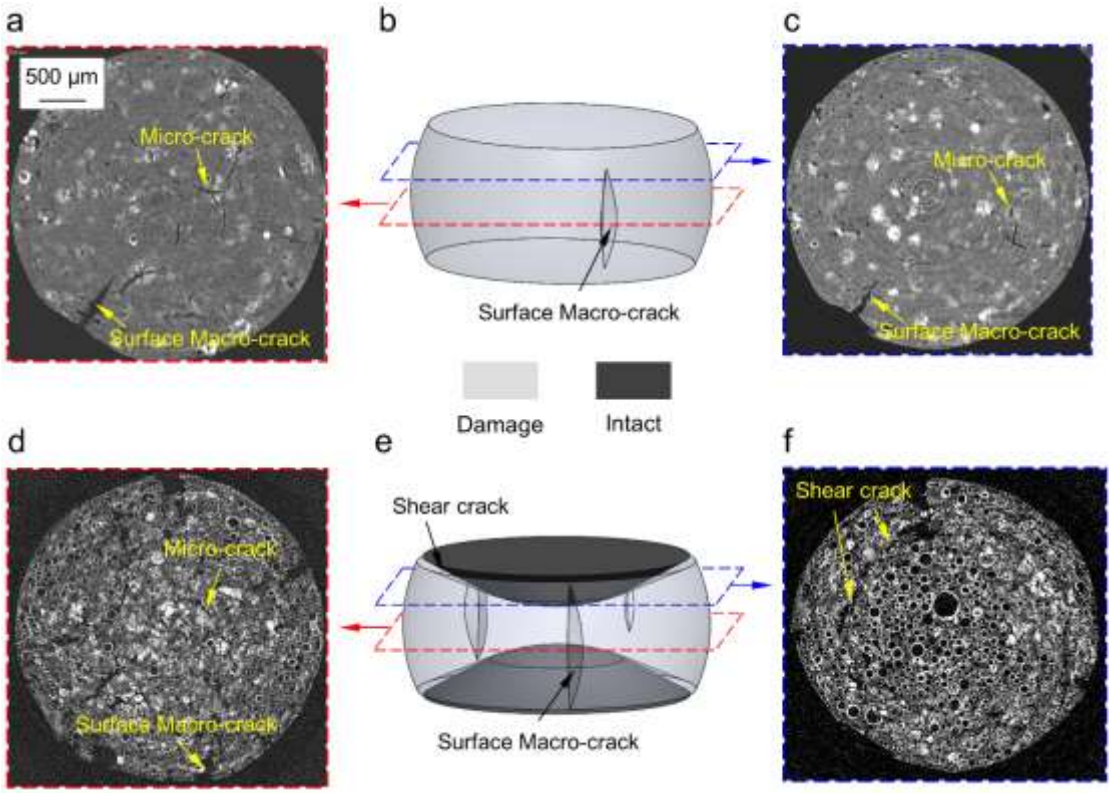

Fig. 5 Syntactic foams with (a–c) low and (d–f) high cenosphere volume fractions: the 3D schematic of matrix cracking failure (b, e), and the typical X-ray microtomographic transverse slices selected from the centre (a, d) and top (c, f) of the two foam specimens (low $V = 0.10$ and high $V = 0.45$) at the strain stage $\varepsilon = 0.5$ during compression.

In the syntactic foam with low V, almost all the cenospheres are crushed in the entire foam specimen at $\varepsilon = 0.5$. The micro-cracks propagating along the external loading direction are mainly distributed in the centre of the specimen (Fig. 5(a)); and a few of them occur in the other portion of the specimen (e.g., Fig. 5(c)). The long

distance between the crushed cenospheres makes the resultant micro-cracks hardly interact with one another. Inspection of all the μXT transverse slices reveals that the individual micro-cracks are localised near the cenospheres even at the large deformation stage $\varepsilon = 0.5$. The lateral tension caused by barrelling in the cylindrical specimen leads to the formation of micro-cracks on the specimen surface. The surface micro-cracks then grow into longitudinal macro-cracks (Fig. 5(a–c)). Further loading in the densification stage can also cause internal micro-cracks to grow and join other micro-cracks to become longitudinal macro-cracks.

Similar to the low *V* syntactic foam, both the surface macro-cracks and internal micro-cracks can be observed in the central transverse slice of the foam with high *V* (Fig. 5(d)). However, the damage is more complex. Due to the short distance between cenospheres in the high *V* foam, micro-cracks can propagate around the neighbouring cenospheres and thus release the stress in these cenospheres. Therefore, some cenospheres remain intact around the internal micro-cracks as shown in Fig. 5(d). As a result of the substantial interaction between cenospheres (and resultant pores), micro-cracks tend to join the adjacent pores or micro-cracks, and grow into macro-cracks longitudinally or diagonally. In particular, the shear stress in the cylindrical specimen can facilitate the evolution of macro-cracks in the diagonal of the specimen. Therefore, an arc-shaped macro-cracks can be observed in the top transverse slice (Fig. 5(f)). The macro-cracks in the diagonal separate the intact zone in the top and bottom of the specimen from the damage zone. As shown in Fig. 5(f), the central portion in the top transverse slice almost remains intact whilst the outer part is damaged.

3.5 Effect of the cenosphere volume fraction on the matrix failure

Prior to crushing of the cenospheres in the syntactic foam, the epoxy matrix holds cenospheres in position and is the constituent to transfer the load, while the cenospheres carry the majority of the applied load. After the cenospheres are fractured, the load carried by the cenospheres is transferred to the neighbouring matrix, and the pores left by the crushed cenospheres act as the stress risers [36].

The finite element model in the previous work [4,12] predicted the stress distribution in the epoxy syntactic foams with different volume fractions of glass microballoons (refer to Fig. 6). The top and bottom of the pore left by the crushed cenosphere are subjected to the highest tensile stress while the equator is under the maximum compressive stress. Note that the epoxy resin is more resistant to compression than to tension or shear. The plastic deformation thus arises near the equator, while matrix micro-cracks tend to initiate in the top and bottom of the crushed cenospheres where the tensile stress concentrates. Therefore, as observed in the foam with low V = 0.10, by the μXT, the micro-cracks initiate and vertically cut through the crushed cenospheres along the loading direction (Fig. 7(a)).

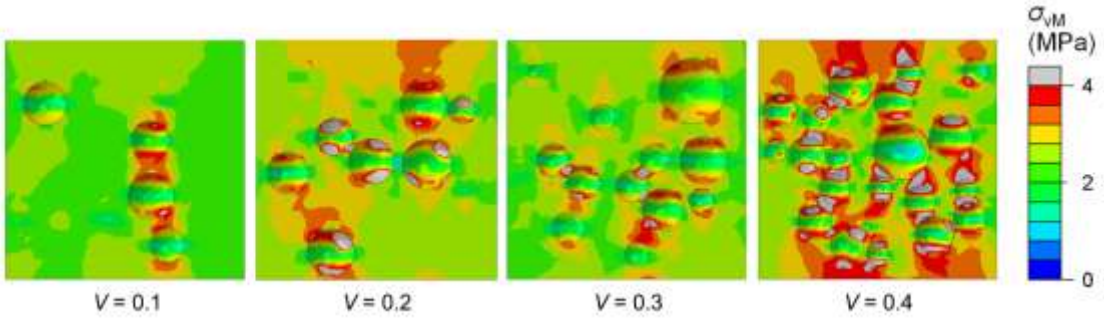

Fig. 6 The predicted von Mises stress distribution in the epoxy matrix of syntactic foams as a function of the glass microballoon volume fraction V [4].

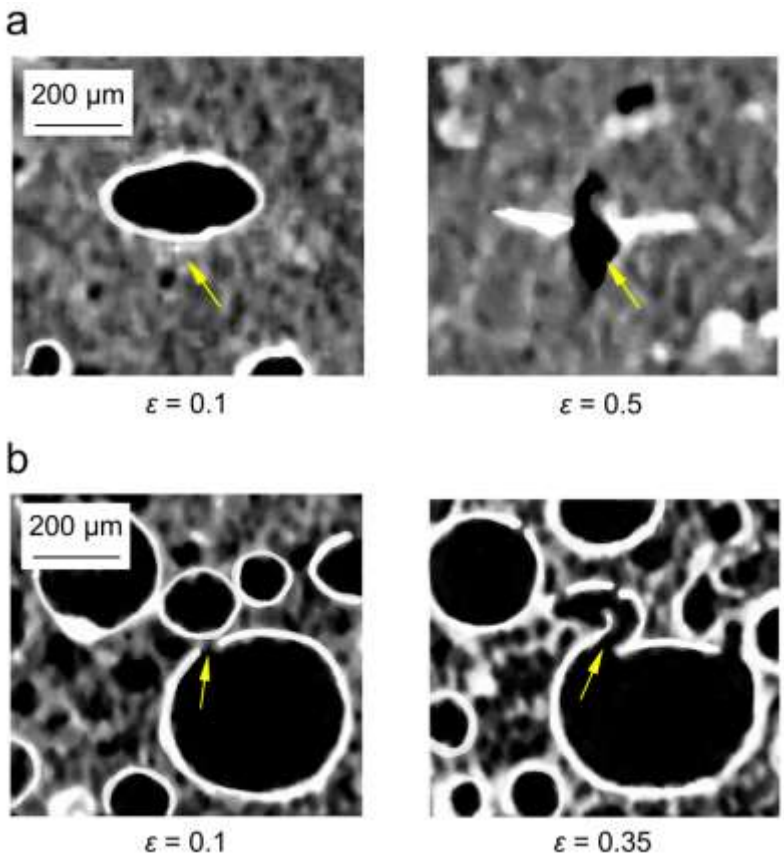

Fig. 7 The X-ray microtomographic longitudinal slices showing typical local matrix micro-cracks in the syntactic foams with the (a) low $V = 0.10$ and (b) high $V = 0.45$ cenosphere volume fractions at two different strain stages.

However, the volume fraction of hollow microspheres significantly influences the stress distribution in the epoxy syntactic foam (Fig. 6). The connection zone between the adjacent cenospheres in the high V foam is also subjected to the high tensile stress after they are crushed. Due to the complicated foam structure and the interaction with cenosphere fragments, the shear stress may also occur in the connection zone. The localised stress strongly depends on the cenosphere size and the distance between the cenospheres. The tensile or shear stress gives rise to the fracture of the epoxy matrix in the connection zone, as observed in the μXT (Fig. 7(b)). After crushing of the adjacent cenospheres, the matrix in the connection zone fractures even at the early strain stage.

4 Conclusions

In-situ μXT of uniaxial compression tests was conducted to investigate the failure process in epoxy syntactic foams with the low and high cenosphere volume fractions (*V*). The CENOSTAR ES500 cenospheres are the constituent to reinforce the epoxy matrix in the syntactic foam. The increased volume fraction of cenospheres improves the initial elastic properties such as Young's modulus and peak strength of the foam. The cenosphere volume fraction has a significant impact on the localised stress and thus the failure mechanism in the matrix around crushed cenospheres due to their distance. In the low *V* foam, micro-cracks initiate in the top and bottom of crushed cenospheres; they propagate longitudinally (along the external loading direction) and join other micro-cracks to become large macro-cracks (longitudinal splitting). Nevertheless, in the high *V* foam, micro-cracks form in the top and bottom of crushed cenospheres as well as near their connection zone, and grow longitudinally and diagonally into macro-cracks in the foam specimen. The present study verifies the proposed mechanism on the effect of the hollow microsphere volume fraction on the matrix failure in syntactic foams, which was elucidated based on the FE modelling in the previous work [4].

Acknowledgements

RH acknowledges the Research Student Scholarship by Nanyang Technological University in Singapore for his PhD study during which this work was carried out.

References

1. Jayavardhan, M. L.; Doddamani, M., *Compos Part B* **2018**, 149, 165.
2. Kumar, B. R. B.; Doddamani, M.; Zeltmann, S. E.; Gupta, N.; Ramesh, M. R.; Ramakrishna, S., *Mater. Des.* **2016**, 92, 414.

3. Yu, W.; Qian, M.; Li, H., *J. Appl. Polym. Sci.* **2016**, 133, 44188..
4. Huang, R.; Li, P., *Compos Part B* **2015**, 78, 401.
5. Li, P.; Petrinic, N.; Siviour, C. R.; Froud, R.; Reed, J. M., *Mater. Sci. Eng., A.* **2009**, 515, 19.
6. Wouterson, E. M.; Boey, F. Y. C.; Hu, X.; Wong, S. C., *Compos. Sci. Technol.* **2005**, 65, 1840.
7. Zhang, L.; Ma, J., *Compos. Sci. Technol.* **2010**, 70, 1265.
8. Labella, M.; Shunmugasamy, V. C.; Strbik, O. M.; Gupta, N., *J. Appl. Polym. Sci.* **2014**, 131, 119.
9. Cochran, J. K., *Curr. Opin. Solid State Mater. Sci.* **1998**, 3, 474.
10. Zhang, Q.; Lee, P. D.; Singh, R.; Wu, G.; Lindley, T. C., *Acta Mater.* **2009**, 57, 3003.
11. Gu, J.; Wu, G.; Zhang, Q., *Scripta Mater.* **2007**, 57, 529.
12. Huang, R.; Li, P.; Liu, T., *Compos. Struct.* **2016**, 140, 157.
13. Huang, R.; Li, P.; Wang, Z.; Liu, T., *Adv. Eng. Mater.* **2016**, 18, 1550.
14. Bharath Kumar, B. R.; Zeltmann, S. E.; Doddamani, M.; Gupta, N.; Gurupadu, S.; Sailaja, R. R. N., *J. Appl. Polym. Sci.* **2016**, 133, 43881.
15. Islam, M. M.; Kim, H. S., *J. Mater. Sci.* **2007**, 42, 6123.
16. Ahmadi, H.; Liaghat, G.; Shokrieh, M.; Hadavinia, H.; Ordys, A.; Aboutorabi, A., *J. Compos. Mater.* **2015**, 49, 1255.
17. Kim, H. S.; Oh, H. H., *J. Appl. Polym. Sci.* **2000**, 76, 1324.
18. Wang, J.; Liang, G.; He, S.; Yang, L., *J. Appl. Polym. Sci.* **2010**, 118, 1252.
19. Woldesenbet, E.; Peter, S., *J. Mater. Sci.* **2009**, 44, 1551.
20. Gupta, N.; Woldesenbet, E.; Mensah, P., *Compos Part A* **2004**, 35, 103.
21. John, B.; Nair, C. P. R.; Devi, K. A.; Ninan, K. N., *J. Mater. Sci.* **2007**, 42, 5398.
22. Kim, H. S.; Plubrai, P., *Compos Part A* **2004**, 35, 1009.
23. Bardella, L.; Perini, G.; Panteghini, A.; Tessier, N.; Gupta, N.; Porfiri, M., *Eur. J. Mech. A-Solid* **2018**, 70C, 58.
24. Shunmugasamy, V. C.; Gupta, N.; Nguyen, N. Q.; Coelho, P. G., *Mater. Sci. Eng., A.* **2015**, 527, 6166.
25. Bardella, L.; Genna, F., *Int. J. Solids. Struct.* **2001**, 38, 7235.
26. Kiser, M.; He, M. Y.; Zok, F. W., *Acta Mater.* **1999**, 47, 2685.
27. Maire, E., *Annu. Rev. Mater. Res.* **2012**, 42, 163.

28. Garcea, S. C.; Sinclair, I.; Spearing, S. M.; Withers, P. J., *Compos. Sci. Technol.* **2017**, 149, 81.
29. Liu, Z.; Li, P.; Srikanth, N.; Liu, T.; Chai, G. B., *Compos Part A* **2016**, 90, 778.
30. Buffiere, J. Y.; Maire, E.; Adrien, J.; Masse, J. P.; Boller, E., *ExM* **2010**, 50, 289.
31. Ohgaki, T.; Toda, H.; Kobayashi, M.; Uesugi, K.; Kobayashi, T.; Niinomi, M.; Akahori, T.; Makii, K.; Aruga, Y., *Adv. Eng. Mater.* **2010**, 8, 473.
32. Ghosh, D.; Wiest, A.; Conner, R. D., *J. Eur. Ceram. Soc.* **2016**, 36, 781.
33. Ho, N. S. K.; Li, P.; Raghavan, S.; Li, T., *Mater. Sci. Eng., A.* **2017**, 687, 123.
34. Li, P.; Nguyen, N. V.; Hao, H., *Mater. Des.* **2016**, 89, 636.
35. Wu, G. H.; Dou, Z. Y.; Sun, D. L.; Jiang, L. T.; Ding, B. S.; He, B. F., *Scripta Mater.* **2007**, 56, 221.
36. Boccaccini, A. R.; Ondracek, G.; Mombello, E., *J. Mater. Sci. Lett.* **1996**, 15, 534.